
Interpretable Lightweight Transformer via Unrolling of Learned Graph Smoothness Priors

Tam Thuc Do
York University
Toronto, Canada
dtamthuc@yorku.ca

Parham Eftekhar
York University
Toronto, Canada
eftekhar@yorku.ca

Seyed Alireza Hosseini
York University
Toronto, Canada
ahosseini@yorku.ca

Gene Cheung
York University
Toronto, Canada
genec@yorku.ca

Philip A. Chou
packet.media
Seattle, USA
pachou@ieee.org

Abstract

We build interpretable and lightweight transformer-like neural networks by unrolling iterative optimization algorithms that minimize graph smoothness priors—the quadratic graph Laplacian regularizer (GLR) and the ℓ_1 -norm graph total variation (GTV)—subject to an interpolation constraint. The crucial insight is that a normalized signal-dependent graph learning module amounts to a variant of the basic self-attention mechanism in conventional transformers. Unlike “black-box” transformers that require learning of large key, query and value matrices to compute scaled dot products as affinities and subsequent output embeddings, resulting in huge parameter sets, our unrolled networks employ shallow CNNs to learn low-dimensional features per node to establish pairwise Mahalanobis distances and construct sparse similarity graphs. At each layer, given a learned graph, the target interpolated signal is simply a low-pass filtered output derived from the minimization of an assumed graph smoothness prior, leading to a dramatic reduction in parameter count. Experiments for two image interpolation applications verify the restoration performance, parameter efficiency and robustness to covariate shift of our graph-based unrolled networks compared to conventional transformers.

1 Introduction

Focusing on the *self-attention* mechanism [1] as the basic building block—where the *affinity* between two input tokens is computed as a scaled dot product—*transformers* [2] learn large parameter sets to achieve state-of-the-art (SOTA) performance in a wide range of signal prediction/classification problems [3, 4], outperforming convolutional neural nets (CNNs) and recurrent neural nets (RNNs). However, there are shortcomings, including i) lack of mathematical interpretability to characterize general performance¹, ii) requiring substantial training datasets to train sizable parameters [12], and iii) fragility to *covariate shift*—when training and testing data have different distributions [13].

Orthogonally, *algorithm unrolling* [14] implements iterations of a model-based algorithm as a sequence of neural layers to build a feed-forward network, whose parameters can be learned end-to-end via back-propagation from data. A classic example is the unrolling of the *iterative soft-thresholding*

¹While works exist to analyze existing transformer architectures [5, 6, 7, 8, 9], only [10, 11] characterized the performance of a single self-attention layer and a shallow transformer, respectively. In contrast, we build transformer-like networks by unrolling graph-based algorithms, so that each layer is interpretable by construction.

algorithm (ISTA) in sparse coding into *Learned* ISTA (LISTA) [15]. Recently, [16] showed that by unrolling an iterative algorithm minimizing a sparse rate reduction (SRR) objective, it can lead to a family of “white-box” transformer-like deep network architectures that are 100% mathematically interpretable. Inspired by [16], in this work we also seek to build white-box transformers via algorithm unrolling, but from a unique *graph signal processing* (GSP) perspective [17, 18, 19].

Over the last decade and a half, GSP studies spectral analysis and processing of discrete signals on structured data kernels described by combinatorial graphs. Specifically, by assuming that the sought signal is smooth (low-pass) with respect to (w.r.t.) a particular graph, a plethora of graph-based restoration algorithms can be designed for practical applications, including image denoising [20], JPEG dequantization [21], interpolation [22], 3D point cloud denoising [23, 24] and super-resolution [25]. At the heart of GSP is the construction of a *similarity graph* that captures pairwise similarities between signal samples on two connected nodes. We first demonstrate that *signal-dependent similarity graph learning with normalization is akin to affinity computation in the self-attention mechanism*. Thus, *our first contribution is to show that unrolling of a graph-based iterative algorithm with normalized graph learning results in an interpretable transformer-like feed-forward network*.

Second, computation of a positive weight $w_{i,j} = \exp(-d(i,j))$ of an edge (i,j) connecting two graph nodes i and j often employs *Mahalanobis distance* $d(i,j) = (\mathbf{f}_i - \mathbf{f}_j)^\top \mathbf{M}(\mathbf{f}_i - \mathbf{f}_j)$ between representative (e.g., CNN-computed) *feature vectors* \mathbf{f}_i and \mathbf{f}_j , where $\mathbf{f}_i, \mathbf{f}_j \in \mathbb{R}^D$ reside in low-dimensional space [26, 27]. Hence, unlike a conventional transformer that requires large key and query matrices, \mathbf{K} and \mathbf{Q} , to compute scaled dot products, the similarity graph learning module can be more parameter-efficient. Moreover, by inserting a graph smoothness prior such as *graph Laplacian regularizer* (GLR) [18, 20] or *graph total variation* (GTV) [28, 29, 30] in the optimization objective, once a graph \mathcal{G} is learned, the target signal is simply computed as the low-pass filtered output derived from the minimization of the assumed graph smoothness prior. Thus, a large value matrix \mathbf{V} to compute output embeddings typical in a transformer is also not needed. *Our second contribution is to demonstrate that a **lightweight** transformer with fewer parameters can be built via unrolling of a graph-based restoration algorithm with a chosen graph signal smoothness prior*.

Specifically, focusing on the signal interpolation problem, we first derive linear-time graph-based algorithms by minimizing GLR or GTV, via *conjugate gradient* (CG) [31] or a modern adaptation of *alternative method of multipliers* (ADMM) for *sparse linear programming* (SLP) [32], respectively. In each iteration, given a learned graph, each algorithm deploys a low-pass graph filter to interpolate the up-sampled observation vector into the target signal. We intersperse unrolled algorithm iterations with graph learning modules into a compact and interpretable neural network. We demonstrate its restoration performance, parameter efficiency (3% of SOTA’s parameters in one case), and robustness to covariate shift for two practical applications: image demosaicking, and image interpolation.

Notation: Vectors and matrices are written in bold lowercase and uppercase letters, respectively. The (i,j) element and the j -th column of a matrix \mathbf{A} are denoted by $A_{i,j}$ and \mathbf{a}_j , respectively. The i -th element in the vector \mathbf{a} is denoted by a_i . The square identity matrix of rank N is denoted by \mathbf{I}_N , the M -by- N zero matrix is denoted by $\mathbf{0}_{M,N}$, and the vector of all ones / zeros of length N is denoted by $\mathbf{1}_N$ / $\mathbf{0}_N$, respectively. Operator $\|\cdot\|_p$ denotes the ℓ - p norm.

2 Preliminaries

A graph $\mathcal{G}(\mathcal{N}, \mathcal{E}, \mathbf{W})$ is defined by a node set $\mathcal{N} = \{1, \dots, N\}$ and an edge set \mathcal{E} of size $|\mathcal{E}| = M$, where $(i,j) \in \mathcal{E}$ means nodes $i, j \in \mathcal{N}$ are connected with weight $w_{i,j} = W_{i,j} \in \mathbb{R}$. In this paper, we consider only *positive* graphs \mathcal{G} with no self-loops, i.e., $w_{i,j} \geq 0, \forall i, j$, and $w_{i,i} = 0, \forall i$. We assume edges are undirected, and thus *adjacency matrix* $\mathbf{W} \in \mathbb{R}^{N \times N}$ is symmetric. The *combinatorial graph Laplacian matrix* is defined as $\mathbf{L} \triangleq \mathbf{D} - \mathbf{W} \in \mathbb{R}^{N \times N}$, where $\mathbf{D} \triangleq \text{diag}(\mathbf{W}\mathbf{1}_N)$ is the *degree matrix*, and $\text{diag}(\mathbf{v})$ returns a diagonal matrix with \mathbf{v} along its diagonal. \mathbf{L} for a positive graph \mathcal{G} is provably *positive semi-definite* (PSD), i.e., all its eigenvalues λ_i ’s are non-negative [19].

We define also the *incidence matrix* $\mathbf{C} = \mathbb{R}^{M \times N}$: each k -th row of \mathbf{C} corresponds to the k -th edge $(i,j) \in \mathcal{E}$, where $C_{k,i} = w_{i,j}$, $C_{k,j} = -w_{i,j}$, and $C_{k,l} = 0, \forall l \neq i, j$. Since our assumed graph \mathcal{G} is undirected, the polarity of $C_{k,i}$ and $C_{k,j}$ are arbitrary, as long as they are opposite.

2.1 Graph Laplacian Regularizer

Given a positive *connected* graph \mathcal{G} with N nodes and M edges, we first define smoothness of a signal $\mathbf{x} \in \mathbb{R}^N$ w.r.t. \mathcal{G} using the *graph Laplacian regularizer* (GLR) [18, 20] as

$$\|\mathbf{x}\|_{\mathcal{G},2} = \mathbf{x}^\top \mathbf{L} \mathbf{x} = \sum_{(i,j) \in \mathcal{E}} w_{i,j} (x_i - x_j)^2 \quad (1)$$

where \mathbf{L} is a combinatorial Laplacian matrix specifying graph \mathcal{G} . GLR (1) is non-negative for a positive graph, and thus is suitable as a signal prior for minimization problems [20, 21].

2.2 Graph Total Variation

Instead of GLR (1), we can alternatively define graph signal smoothness via *graph total variation* (GTV) [28, 29, 30] $\|\mathbf{x}\|_{\mathcal{G},1}$ for signal $\mathbf{x} \in \mathbb{R}^N$ as

$$\|\mathbf{x}\|_{\mathcal{G},1} = \|\mathbf{C}\mathbf{x}\|_1 \stackrel{(a)}{=} \sum_{(i,j) \in \mathcal{E}} w_{i,j} |x_i - x_j| \quad (2)$$

where (a) is true since \mathcal{G} is positive. GTV is also non-negative for positive \mathcal{G} , and has been used as a signal prior for restoration problems such as image deblurring [33].

3 Problem Formulation & Optimization using GLR

3.1 Problem Formulation

We first assume a positive, *sparse* and *connected* graph \mathcal{G} with N nodes and M edges specified by graph Laplacian matrix \mathbf{L} . By sparse, we mean that M is $\mathcal{O}(N)$ and not $\mathcal{O}(N^2)$. By connected, we mean that any node j can be traversed from any other node i . Given \mathcal{G} , we first derive an iterative algorithm to interpolate signal \mathbf{x} by minimizing GLR given observed samples \mathbf{y} . In Section 4, we derive an algorithm by minimizing GTV instead given \mathbf{y} . In Section 5, we unroll iterations of one of two derived algorithms into neural layers, together with strategically inserted graph learning modules, to construct graph-based lightweight transformer-like neural nets.

We first employ GLR [20] as the objective to reconstruct $\mathbf{x} \in \mathbb{R}^N$ given partial observation $\mathbf{y} \in \mathbb{R}^K$, where $K < N$. Denote by $\mathbf{H} \in \{0, 1\}^{K \times N}$ a *sampling matrix* defined as

$$H_{i,j} = \begin{cases} 1 & \text{if node } j \text{ is the } i\text{-th sample} \\ 0 & \text{o.w.} \end{cases} \quad (3)$$

that picks out K samples from signal \mathbf{x} . The optimization is thus

$$\min_{\mathbf{x}} \mathbf{x}^\top \mathbf{L} \mathbf{x}, \quad \text{s.t. } \mathbf{H}\mathbf{x} = \mathbf{y} \quad (4)$$

where $\mathbf{L} \in \mathbb{R}^{N \times N}$ is a graph Laplacian matrix corresponding to a positive graph \mathcal{G} [19]. PSD \mathbf{L} implies that $\mathbf{x}^\top \mathbf{L} \mathbf{x} \geq 0, \forall \mathbf{x}$, and thus (4) has a convex objective with a linear interpolation constraint.

3.2 Optimization

We solve (4) via a standard Lagrangian approach [34] and write its corresponding unconstrained Lagrangian function $f(\mathbf{x}, \boldsymbol{\mu})$ as

$$f(\mathbf{x}, \boldsymbol{\mu}) = \mathbf{x}^\top \mathbf{L} \mathbf{x} + \boldsymbol{\mu}^\top (\mathbf{H}\mathbf{x} - \mathbf{y}) \quad (5)$$

where $\boldsymbol{\mu} \in \mathbb{R}^K$ is the Lagrange multiplier vector. To minimize $f(\mathbf{x}, \boldsymbol{\mu})$ in (5), we take the derivative w.r.t. \mathbf{x} and $\boldsymbol{\mu}$ separately and set them to zero, resulting in the following linear system:

$$\underbrace{\begin{bmatrix} 2\mathbf{L} & \mathbf{H}^\top \\ \mathbf{H} & \mathbf{0}_{K,K} \end{bmatrix}}_{\mathbf{P}} \begin{bmatrix} \mathbf{x} \\ \boldsymbol{\mu} \end{bmatrix} = \begin{bmatrix} \mathbf{0}_{N,N} \\ \mathbf{y} \end{bmatrix}. \quad (6)$$

Given that the underlying graph \mathcal{G} is positive and connected, coefficient matrix \mathbf{P} is provably full-rank and thus invertible (see Appendix A.1 for a proof). Hence, (6) has a unique solution \mathbf{x}^* .

Suppose we index the sampled nodes \mathcal{S} in \mathbf{x} before the non-sampled nodes $\bar{\mathcal{S}}$, *i.e.*, $\mathbf{x} = [\mathbf{x}_{\mathcal{S}}; \mathbf{x}_{\bar{\mathcal{S}}}]$. Then $\mathbf{H} = [\mathbf{I}_K \ \mathbf{0}_{K, N-K}]$, and the second block row in (6) implies $\mathbf{x}_{\mathcal{S}} = \mathbf{y}$. Suppose we write $\mathbf{L} = [\mathbf{L}_{\mathcal{S}, \mathcal{S}} \ \mathbf{L}_{\mathcal{S}, \bar{\mathcal{S}}}; \mathbf{L}_{\bar{\mathcal{S}}, \mathcal{S}} \ \mathbf{L}_{\bar{\mathcal{S}}, \bar{\mathcal{S}}}]$ in blocks also. For the first block row in (6), consider only the non-sampled rows:

$$\left(\begin{bmatrix} 2\mathbf{L} & \mathbf{H}^\top \end{bmatrix} \begin{bmatrix} \mathbf{x} \\ \boldsymbol{\mu} \end{bmatrix} \right)_{\bar{\mathcal{S}}} = 2(\mathbf{L}_{\bar{\mathcal{S}}, \mathcal{S}} \mathbf{x}_{\mathcal{S}} + \mathbf{L}_{\bar{\mathcal{S}}, \bar{\mathcal{S}}} \mathbf{x}_{\bar{\mathcal{S}}}) = \mathbf{0}_{N-K} \quad (7)$$

where $(\mathbf{H}^\top \boldsymbol{\mu})_{\bar{\mathcal{S}}} = \mathbf{0}_{N-K}$ since the non-sampled rows of \mathbf{H}^\top (the non-sampled columns of \mathbf{H}) are zeros. Thus, $\mathbf{x}_{\bar{\mathcal{S}}}$ can be computed via the following system of linear equations:

$$\mathbf{L}_{\bar{\mathcal{S}}, \bar{\mathcal{S}}} \mathbf{x}_{\bar{\mathcal{S}}} = -\mathbf{L}_{\bar{\mathcal{S}}, \mathcal{S}} \mathbf{y} \quad (8)$$

where $\mathbf{L}_{\bar{\mathcal{S}}, \bar{\mathcal{S}}}$ is a symmetric, sparse, and provably *positive definite* (PD) matrix (see Appendix A.2 for a proof). Thus, there exists a unique solution $\mathbf{x}_{\bar{\mathcal{S}}}$ in (8).

Complexity: For notation simplicity, let $\mathcal{L} = \mathbf{L}_{\bar{\mathcal{S}}, \bar{\mathcal{S}}}$. Linear system (8) can be solved efficiently using *conjugate gradient* (CG), an iterative descent algorithm with complexity $\mathcal{O}(\text{nnz}(\mathcal{L})\sqrt{\kappa(\mathcal{L})}/\log(\epsilon))$, where $\text{nnz}(\mathcal{L})$ is the number of non-zero entries in matrix \mathcal{L} , $\kappa(\mathcal{L}) = \frac{\lambda_{\max}(\mathcal{L})}{\lambda_{\min}(\mathcal{L})}$ is the *condition number* of \mathcal{L} , $\lambda_{\max}(\mathcal{L})$ and $\lambda_{\min}(\mathcal{L})$ are the respective largest and smallest eigenvalues of \mathcal{L} , and ϵ is the convergence threshold of the gradient search [31]. Because \mathbf{L} is sparse by graph construction ($\mathcal{O}(N)$ edges), $\mathcal{L} = \mathbf{L}_{\bar{\mathcal{S}}, \bar{\mathcal{S}}}$ is also sparse, *i.e.*, $\text{nnz}(\mathcal{L}) = \mathcal{O}(N)$. Assuming $\kappa(\mathcal{L})$ can be reasonably lower-bounded for PD \mathcal{L} and ϵ is reasonably chosen, the complexity of solving (8) using CG is $\mathcal{O}(N)$.

Interpretation: To elicit a signal filtering interpretation from (6), we assume for now that \mathbf{L} is PD² and thus invertible. Recall that the block matrix inversion formula [35] is

$$\mathbf{P}^{-1} = \left(\begin{bmatrix} \mathbf{A} & \mathbf{B} \\ \mathbf{C} & \mathbf{D} \end{bmatrix} \right)^{-1} = \begin{bmatrix} \mathbf{A}^{-1} + \mathbf{A}^{-1}\mathbf{B}(\mathbf{P}/\mathbf{A})\mathbf{C}\mathbf{A}^{-1} & -\mathbf{A}^{-1}\mathbf{B}(\mathbf{P}/\mathbf{A}) \\ -(\mathbf{P}/\mathbf{A})\mathbf{C}\mathbf{A}^{-1} & (\mathbf{P}/\mathbf{A}) \end{bmatrix} \quad (9)$$

where $\mathbf{P}/\mathbf{A} = (\mathbf{D} - \mathbf{C}\mathbf{A}^{-1}\mathbf{B})^{-1}$ is the *Schur complement* of block \mathbf{A} of matrix \mathbf{P} . Solution \mathbf{x}^* can thus be computed as:

$$\begin{aligned} \mathbf{x}^* &= \mathbf{L}^{-1}\mathbf{H}^\top (\mathbf{H}\mathbf{L}^{-1}\mathbf{H}^\top)^{-1} \mathbf{y} \\ &= \mathbf{L}^{-1}\mathbf{H}^\top ((\mathbf{L}^{-1})_{\mathcal{S}})^{-1} \mathbf{y} = \mathbf{L}^{-1}\mathbf{H}^\top \mathbf{L}_{\mathcal{S}}^\# \mathbf{y} \end{aligned} \quad (10)$$

where $\mathbf{L}_{\mathcal{S}}^\# \triangleq ((\mathbf{L}^{-1})_{\mathcal{S}})^{-1}$ and $(\mathbf{L}^{-1})_{\mathcal{S}}$ denotes the rows and columns of \mathbf{L}^{-1} corresponding to the sampled nodes. $\mathbf{L}_{\mathcal{S}}^\#$ is a high-pass filter similar to $\mathbf{L}_{\mathcal{S}}$. Thus, we can interpret \mathbf{x}^* as a *low-pass filtered output of up-sampled* $\mathbf{H}^\top \mathbf{L}_{\mathcal{S}}^\# \mathbf{y}$ —with low-pass filter response $r(\boldsymbol{\Lambda}) = \boldsymbol{\Lambda}^{-1}$ where $\mathbf{L} = \mathbf{V}\boldsymbol{\Lambda}\mathbf{V}^\top$, $\boldsymbol{\Lambda} = \text{diag}([\lambda_1, \dots, \lambda_N])$, is eigen-decomposable with frequencies λ_k 's and Fourier modes \mathbf{v}_k 's.

4 Problem Formulation & Optimization using GTV

4.1 Problem Formulation

Given a positive connected graph \mathcal{G} specified by incidence matrix $\mathbf{C} \in \mathbb{R}^{M \times N}$ and partial observation \mathbf{y} , we now employ instead GTV as the objective to interpolate target signal \mathbf{x} , resulting in

$$\min_{\mathbf{x}} \|\mathbf{C}\mathbf{x}\|_1, \quad \text{s.t. } \mathbf{H}\mathbf{x} = \mathbf{y}, \quad (11)$$

(11) is a *linear program* (LP), since both the objective and the lone constraint are linear. Thus, while minimizing GLR leads to a *linear system* (6), minimizing GTV leads to a *linear program* (11).

²A combinatorial graph Laplacian matrix for a positive graph with at least one additional positive self-loop is provably PD; see proof in Appendix A.2.

4.1.1 LP in Standard Form

First, we rewrite LP (11) in standard form as follows. Define *upper-bound variable* $\mathbf{z} \in \mathbb{R}^M$ with a pair of linear constraints $\mathbf{z} \geq \pm \mathbf{C}\mathbf{x}$. This enables a linear objective $\mathbf{1}_M^\top \mathbf{z}$ for a minimization problem (thus ensuring the upper bound is tight), *i.e.*, $\mathbf{z} = \|\mathbf{C}\mathbf{x}\|_1$. Second, we introduce non-negative *slack variables* $\mathbf{q}_1, \mathbf{q}_2 \in \mathbb{R}^M$ to convert inequality constraints $\mathbf{z} \geq \pm \mathbf{C}\mathbf{x}$ to equality constraints $\mathbf{z} = \mathbf{C}\mathbf{x} + \mathbf{q}_1$ and $\mathbf{z} = -\mathbf{C}\mathbf{x} + \mathbf{q}_2$. Thus, LP (11) can be rewritten as

$$\min_{\mathbf{z}, \mathbf{x}, \mathbf{q}} \mathbf{1}_M^\top \mathbf{z}, \quad \text{s.t.} \quad \underbrace{\begin{bmatrix} \mathbf{I}_M & -\mathbf{C} & -(\mathbf{I}_M \ \mathbf{0}_{M,M}) \\ \mathbf{I}_M & \mathbf{C} & -(\mathbf{0}_{M,M} \ \mathbf{I}_M) \\ \mathbf{0}_{K,M} & \mathbf{H} & \mathbf{0}_{K,2M} \end{bmatrix}}_{\mathbf{A}} \begin{bmatrix} \mathbf{z} \\ \mathbf{x} \\ \mathbf{q} \end{bmatrix} = \underbrace{\begin{bmatrix} \mathbf{0}_M \\ \mathbf{0}_M \\ \mathbf{y} \end{bmatrix}}_{\mathbf{b}}, \quad \mathbf{q} \geq \mathbf{0}_{2M} \quad (12)$$

where $\mathbf{q} = [\mathbf{q}_1; \mathbf{q}_2] \in \mathbb{R}^{2M}$.

4.2 Optimization Algorithm

Because coefficient matrix \mathbf{A} is sparse, (12) is a *sparse linear program* (SLP). We solve SLP (12) efficiently by adopting an ADMM approach for SLP in [32]. We first define a convex but non-differentiable (non-smooth) *indicator function*:

$$g(\mathbf{q}) = \begin{cases} 0 & \text{if } q_j \geq 0, \forall j \\ \infty & \text{o.w.} \end{cases}. \quad (13)$$

We next introduce *auxiliary variable* $\tilde{\mathbf{q}} \in \mathbb{R}^{2M}$ and equality constraint $\tilde{\mathbf{q}} = \mathbf{q}$. We now rewrite (12) with a single equality constraint as

$$\min_{\mathbf{z}, \mathbf{x}, \mathbf{q}, \tilde{\mathbf{q}}} \mathbf{1}_M^\top \mathbf{z} + g(\tilde{\mathbf{q}}), \quad \text{s.t.} \quad \underbrace{\begin{bmatrix} \mathbf{A} & \\ \mathbf{0}_{2M, M+N} & \mathbf{I}_{2M} \end{bmatrix}}_{\mathbf{B}} \begin{bmatrix} \mathbf{z} \\ \mathbf{x} \\ \mathbf{q} \end{bmatrix} = \begin{bmatrix} \mathbf{b} \\ \tilde{\mathbf{q}} \end{bmatrix}. \quad (14)$$

We can now rewrite (14) into an unconstrained version using the augmented Lagrangian method as

$$\min_{\mathbf{z}, \mathbf{x}, \mathbf{q}, \tilde{\mathbf{q}}} \mathbf{1}_M^\top \mathbf{z} + g(\tilde{\mathbf{q}}) + \boldsymbol{\mu}^\top \left(\mathbf{B} \begin{bmatrix} \mathbf{z} \\ \mathbf{x} \\ \mathbf{q} \end{bmatrix} - \begin{bmatrix} \mathbf{b} \\ \tilde{\mathbf{q}} \end{bmatrix} \right) + \frac{\gamma}{2} \left\| \mathbf{B} \begin{bmatrix} \mathbf{z} \\ \mathbf{x} \\ \mathbf{q} \end{bmatrix} - \begin{bmatrix} \mathbf{b} \\ \tilde{\mathbf{q}} \end{bmatrix} \right\|_2^2 \quad (15)$$

where $\boldsymbol{\mu} \in \mathbb{R}^{4M+K}$ is a Lagrange multiplier vector, and $\gamma > 0$ is a scalar parameter. In the sequel, we write $\boldsymbol{\mu} = [\boldsymbol{\mu}_a; \boldsymbol{\mu}_b; \boldsymbol{\mu}_c; \boldsymbol{\mu}_d; \boldsymbol{\mu}_e]$, where $\boldsymbol{\mu}_a, \boldsymbol{\mu}_b, \boldsymbol{\mu}_d, \boldsymbol{\mu}_e \in \mathbb{R}^M$ and $\boldsymbol{\mu}_c \in \mathbb{R}^K$.

4.2.1 Optimizing Main Variables

As typically done in ADMM, we minimize the unconstrained objective (15) alternately as follows. At iteration t , when $\tilde{\mathbf{q}}^t$ and $\boldsymbol{\mu}^t$ are fixed, the optimization for \mathbf{z}^{t+1} , \mathbf{x}^{t+1} and \mathbf{q}^{t+1} becomes

$$\min_{\mathbf{z}, \mathbf{x}, \mathbf{q}} \mathbf{1}_M^\top \mathbf{z} + (\boldsymbol{\mu}^t)^\top \left(\mathbf{B} \begin{bmatrix} \mathbf{z} \\ \mathbf{x} \\ \mathbf{q} \end{bmatrix} - \begin{bmatrix} \mathbf{b} \\ \tilde{\mathbf{q}} \end{bmatrix} \right) + \frac{\gamma}{2} \left\| \mathbf{B} \begin{bmatrix} \mathbf{z} \\ \mathbf{x} \\ \mathbf{q} \end{bmatrix} - \begin{bmatrix} \mathbf{b} \\ \tilde{\mathbf{q}} \end{bmatrix} \right\|_2^2. \quad (16)$$

The solution to this convex and smooth quadratic optimization is a system of linear equations,

$$\mathbf{z}^{t+1} = -\frac{1}{\gamma} \mathbf{1}_M - \frac{1}{2\gamma} (\boldsymbol{\mu}_a^t + \boldsymbol{\mu}_b^t + \boldsymbol{\mu}_d^t + \boldsymbol{\mu}_e^t) + \frac{1}{2} (\tilde{\mathbf{q}}_1^t + \tilde{\mathbf{q}}_2^t) \quad (17)$$

$$(\mathbf{C}^\top \mathbf{C} + \mathbf{H}^\top \mathbf{H}) \mathbf{x}^{t+1} = \frac{1}{2\gamma} \mathbf{C}^\top (\boldsymbol{\mu}_a^t - \boldsymbol{\mu}_b^t + \boldsymbol{\mu}_d^t - \boldsymbol{\mu}_e^t) - \frac{1}{\gamma} \mathbf{H}^\top \boldsymbol{\mu}_c^t - \frac{1}{2} \mathbf{C}^\top (\tilde{\mathbf{q}}_1^t - \tilde{\mathbf{q}}_2^t) + \mathbf{H}^\top \mathbf{y} \quad (18)$$

$$\mathbf{q}_1^t = \frac{1}{2} (\mathbf{z}^{t+1} - \mathbf{C}\mathbf{x}^{t+1}) + \frac{1}{2\gamma} (\boldsymbol{\mu}_a^t - \boldsymbol{\mu}_d^t + \gamma \tilde{\mathbf{q}}_1^t)$$

$$\mathbf{q}_2^t = \frac{1}{2} (\mathbf{z}^{t+1} + \mathbf{C}\mathbf{x}^{t+1}) + \frac{1}{2\gamma} (\boldsymbol{\mu}_b^t - \boldsymbol{\mu}_e^t + \gamma \tilde{\mathbf{q}}_2^t) \quad (19)$$

See the Appendix A.3 for a derivation.

Linear system (18) is solvable if the coefficient matrix $\mathcal{L} \triangleq \mathbf{L} + \mathbf{H}^\top \mathbf{H}$, where $\mathbf{L} \triangleq \mathbf{C}^\top \mathbf{C}$ is a PSD graph Laplacian for a positive graph, is invertible. See Appendix A.4 for a proof that \mathcal{L} is PD and thus invertible.

Complexity: Linear system (18) again can be solved efficiently using CG with complexity $\mathcal{O}(\text{nnz}(\mathcal{L})\sqrt{\kappa(\mathcal{L})}/\log(\epsilon))$ [31]. Because \mathbf{C} is sparse by graph construction ($\mathcal{O}(N)$ edges) and \mathbf{H} is sparse by definition, \mathcal{L} is also sparse, *i.e.*, $\text{nnz}(\mathcal{L}) = \mathcal{O}(N)$. Thus, assuming $\kappa(\mathcal{L})$ is also upper-bounded and ϵ is reasonably chosen, the complexity of solving (18) using CG is $\mathcal{O}(N)$.

Interpretation: (18) can be interpreted as follows. $\mathbf{H}^\top \mathbf{y}$ is the *up-sampled version* of observation \mathbf{y} . $\mathcal{L} = \mathbf{V}\mathbf{\Lambda}\mathbf{V}^\top$, $\mathbf{\Lambda} = \text{diag}([\lambda_1, \dots, \lambda_N])$, is an eigen-decomposable *generalized Laplacian matrix*—Laplacian matrix $\mathbf{C}^\top \mathbf{C}$ plus self-loops of weight 1 at sampled nodes due to diagonal matrix $\mathbf{H}^\top \mathbf{H}$, and like a graph Laplacian \mathbf{L} without self-loops, can be interpreted as a high-pass spectral filter [36]. $\mathcal{L}^{-1} = \mathbf{V}\mathbf{\Lambda}^{-1}\mathbf{V}^\top$ is thus a *low-pass* spectral filter with frequency response $r(\mathbf{\Lambda}) = \mathbf{\Lambda}^{-1}$ to interpolate output $\mathcal{L}^{-1}\mathbf{H}^\top \mathbf{y}$. We interpret the remaining terms on the right-hand side of (18) as bias.

4.2.2 Optimizing Auxiliary Variable

Fixing \mathbf{z}^{t+1} , \mathbf{x}^{t+1} and \mathbf{q}^{t+1} , the optimization for $\tilde{\mathbf{q}}^{t+1}$ for (15) simplifies to

$$\min_{\tilde{\mathbf{q}}} g(\tilde{\mathbf{q}}) + (\boldsymbol{\mu}_d^t)^\top (\mathbf{q}^{t+1} - \tilde{\mathbf{q}}) + \frac{\gamma}{2} \|\mathbf{q}^{t+1} - \tilde{\mathbf{q}}\|_2^2. \quad (20)$$

The solution for optimal $\tilde{\mathbf{q}}^{t+1}$ is term-by-term thresholding:

$$\tilde{q}_i^{t+1} = \begin{cases} q_i^{t+1} + \frac{1}{\gamma} \mu_{d,i}^t & \text{if } q_i^{t+1} + \frac{1}{\gamma} \mu_{d,i}^t \geq 0 \\ 0 & \text{o.w.} \end{cases}, \forall i. \quad (21)$$

See Appendix A.5 for a derivation.

4.2.3 Updating Lagrange Multiplier

The Lagrange multiplier $\boldsymbol{\mu}^{t+1}$ can be updated in the usual manner in an ADMM framework [37]:

$$\boldsymbol{\mu}^{t+1} = \boldsymbol{\mu}^t + \gamma \left(\mathbf{B} \begin{bmatrix} \mathbf{z} \\ \mathbf{x} \\ \mathbf{q} \end{bmatrix} - \begin{bmatrix} \mathbf{b} \\ \tilde{\mathbf{q}} \end{bmatrix} \right). \quad (22)$$

Algorithm Complexity: Given that the number of iterations until ADMM convergence is not a function of input size, it is $\mathcal{O}(1)$. The most time-consuming step in each ADMM iteration is the solving of linear system (18) via CG in $\mathcal{O}(N)$. Thus, we conclude that solving SLP (12) using the aforementioned ADMM algorithm is $\mathcal{O}(N)$.

Algorithm Comparison: Comparing the CG algorithm used to solve linear system (8) and the ADMM algorithm developed to solve SLP (12), we first observe that, given a similarity graph \mathcal{G} specified by Laplacian or incidence matrix, \mathbf{L} or \mathbf{C} , both algorithms compute the interpolated signal \mathbf{x}^* as a low-pass filtered output of the up-sampled input $\mathbf{H}^\top \mathbf{y}$ in (10) and (18), respectively. This is intuitive, given the assumed graph smoothness priors, GLR and GTV. We see also that the ADMM algorithm is more intricate: in each iteration, the main variables are computed using CG, while the auxiliary variable is updated via ReLU-like thresholding. As a result, the ADMM algorithm is more amenable to deep algorithm unrolling with better performance in general (see Section 6 for details).

5 Graph Learning & Algorithm Unrolling

We now discuss how a similarity graph \mathcal{G} can be learned from data, specified as graph Laplacian \mathbf{L} for GLR minimization (4) or incidence matrix \mathbf{C} for GTV minimization (11), so that the two proposed graph-based interpolations can take place. Moreover, we show how a normalized graph learning module³ performs comparable operations to the self-attention mechanism in conventional transformers. Thus, unrolling sequential pairs of graph-based iterative algorithm and graph learning module back-to-back leads to an interpretable “white-box” transformer-like neural net.

³While estimating a precision (graph Laplacian) matrix from an empirical covariance matrix computed from data is another graph learning approach [38, 39, 40], we pursue a feature-based approach here [26, 27].

5.1 Self-Attention Operator in Transformer

We first review the self-attention operator in a conventional transformer architecture, defined using a scaled dot product and a softmax operation [1]. Specifically, first denote by $\mathbf{x}_i \in \mathbb{R}^E$ an *embedding* for token i of N tokens. *Affinity* $e(i, j)$ between tokens i and j is defined as the dot product between linear-transformed embeddings $\mathbf{K}\mathbf{x}_i$ and $\mathbf{Q}\mathbf{x}_j$, where $\mathbf{Q}, \mathbf{K} \in \mathbb{R}^{E \times E}$ are the *query* and *key* matrices, respectively. Using softmax, a non-linear function that maps a vector of real numbers to a vector of positive numbers that sum to 1, *attention weight* $a_{i,j}$ is computed as

$$a_{i,j} = \frac{\exp(e(i, j))}{\sum_{l=1}^N \exp(e(i, l))}, \quad e(i, j) = (\mathbf{Q}\mathbf{x}_j)^\top (\mathbf{K}\mathbf{x}_i). \quad (23)$$

Given self-attention coefficients $a_{i,j}$, output embedding \mathbf{y}_i for token i is computed as

$$\mathbf{y}_i = \sum_{l=1}^N a_{i,l} \mathbf{x}_l \mathbf{V} \quad (24)$$

where $\mathbf{V} \in \mathbb{R}^{E \times E}$ is a *value* matrix. ‘‘Self-attention’’ here means that input embeddings are weighted to compute output embeddings. A transformer is thus a sequence of embedding-to-embedding mappings via different learned self-attention operations defined by \mathbf{Q}, \mathbf{K} and \mathbf{V} matrices. *Multi-head* attention is possible when multiple query and key matrices $\mathbf{Q}^{(m)}$ and $\mathbf{K}^{(m)}$ are used to compute different attention weights $a_{i,j}^{(m)}$ ’s for the same input embeddings \mathbf{x}_i and \mathbf{x}_j , and the output embedding \mathbf{y}_i is computed using an average of these multi-head attention weights $a_{i,l}^{(m)}$ ’s.

5.2 Computation of Graph Edge Weights

Consider now how edge weights $w_{i,j}$ ’s can be computed from data to specify a combinatorial graph \mathcal{G} [26, 27]. A low-dimensional *feature vector* $\mathbf{f}_i \in \mathbb{R}^D$ can be computed for each node i from embedding $\mathbf{e}_i \in \mathbb{R}^E$ via some (possibly non-linear) function $\mathbf{f}_i = F(\mathbf{e}_i)$, where typically $D \ll E$. Edge weight $w_{i,j}$ between nodes i and j in a graph \mathcal{G} can then be computed as

$$w_{i,j} = \exp(-d(i, j)), \quad d(i, j) = (\mathbf{f}_i - \mathbf{f}_j)^\top \mathbf{M} (\mathbf{f}_i - \mathbf{f}_j) \quad (25)$$

where $d(i, j)$ is the squared *Mahalanobis distance* given PSD *metric matrix* \mathbf{M} that quantifies the difference between nodes i and j . M edge weights $\{w_{i,j}\}$ compose a graph \mathcal{G} , specified by the Laplacian matrix \mathbf{L} for GLR minimization (4) and the incidence matrix $\mathbf{C}^{M \times N}$ for GTV minimization (11). Because $w_{i,j} \geq 0, \forall i, j$, constructed graph \mathcal{G} is positive.

As a concrete example, consider *bilateral filter* (BF) weights commonly used in image filtering [41], where feature \mathbf{f}_i contains the 2D grid location \mathbf{l}_i and color intensity x_i of pixel i , and metric $\mathbf{M} = \text{diag}([1/\sigma_d^2; 1/\sigma_r^2])$ is a diagonal matrix with weights to specify the relative strength of the *domain* and *range* filters in BF. Because BF uses input pixel intensities x_l ’s to compute weighted output pixel intensities x_i ’s, BF is *signal-dependent*, similar to self-attention weights in transformers.

Edge weights are often first *normalized* before being used for filtering.

Normalization: For normalization, the symmetric *normalized graph Laplacian* \mathbf{L}_n is defined as $\mathbf{L}_n \triangleq \mathbf{D}^{-1/2} \mathbf{L} \mathbf{D}^{-1/2}$, so that the diagonal entries of \mathbf{L}_n are all ones (assuming \mathcal{G} is connected and positive) [18]. We assume normalized \mathbf{L}_n is used for Laplacian \mathbf{L} in GLR minimization in (4).

Alternatively, the asymmetric *random walk graph Laplacian* \mathbf{L}_{rw} is defined as $\mathbf{L}_{rw} \triangleq \mathbf{D}^{-1} \mathbf{L}$, so that the sum of each row of \mathbf{L}_{rw} equals to zero [18]. Interpreting \mathbf{L}_{rw} as a Laplacian matrix to a *directed* graph, the weight sum of edges leaving each node i is one, *i.e.*, $\sum_{l|(i,l) \in \mathcal{E}} \bar{w}_{i,l} = 1, \forall i$. To accomplish this, undirected edges weights $\{w_{i,j}\}$ are normalized to $\{\bar{w}_{i,j}\}$ via

$$\bar{w}_{i,j} = \frac{\exp(-d(i, j))}{\sum_{l|(i,l) \in \mathcal{E}} \exp(-d(i, l))}. \quad (26)$$

For GTV minimization in (11), we normalize edge weights in incidence matrix \mathbf{C} instead using (26). This results in normalized $\bar{\mathbf{C}} \in \mathbb{R}^{2M \times N}$ for a *directed* graph with $2M$ directed edges. Subsequently,

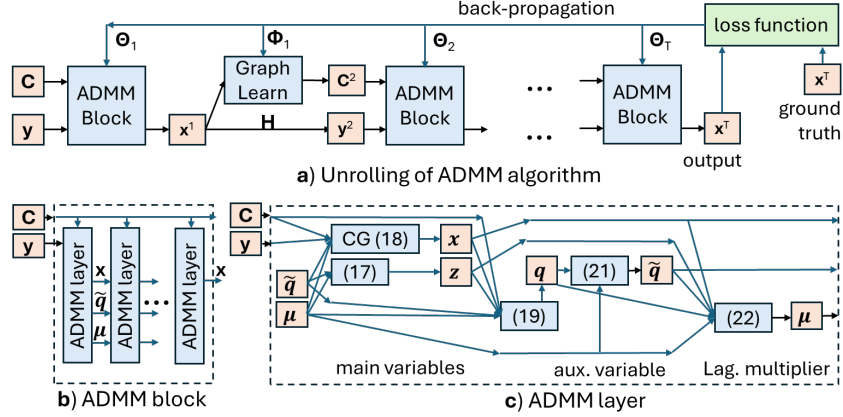


Figure 1: Unrolling of GTV-based signal interpolation algorithm.

we define symmetric graph Laplacian $\bar{\mathbf{L}} = \bar{\mathbf{C}}^\top \bar{\mathbf{C}}$ and generalized graph Laplacian $\bar{\mathcal{L}} = \bar{\mathbf{L}} + \mathbf{H}^\top \mathbf{H}$. Note that $\|\bar{\mathbf{C}}\mathbf{1}\|_1 = \sum_{l=1}^N \bar{w}_{i,l} |1 - 1| = 0$ after normalization, as expected for a total variation term on a constant signal $\mathbf{1}$. Further, note that while $\bar{\mathbf{C}}$ is an incidence matrix for a directed graph with $2M$ edges, $\bar{\mathbf{L}}$ is a graph Laplacian for an undirected graph with M edges. See Fig. 3 in Appendix A.6 for an example of incidence matrix $\bar{\mathbf{C}}$, normalized incidence matrix $\bar{\mathbf{C}}$, and graph Laplacian matrix $\bar{\mathbf{L}}$.

Comparison to Self-Attention Operator: We see how the definitions of edge weights (25) and normalization (26) are similar to attention weights in (23). Specifically, *interpreting the negative squared Mahalanobis distance $-d(i, j)$ as affinity $e(i, j)$, normalized edge weights $\bar{w}_{i,j}$ in (25) are essentially the same as attention weights $a_{i,j}$ in (23)*. The only differences are: i) how non-negative Mahalanobis distance $d(i, j)$ is computed in (25) using features $\mathbf{f}_i = F(\mathbf{e}_i)$ and metric \mathbf{M} versus how real-valued affinity is computed via a dot product in (23), and ii) how the normalization term is computed in a one-hop neighborhood from node i in (26) versus how it is computed using all N tokens in (23). These details have complexity implications, which we will revisit in the sequel.

Further, we note that, given a graph \mathcal{G} , the interpolated signal \mathbf{x}^* is computed simply as a low-pass filtered output of the up-sampled input observation $\mathbf{H}^\top \mathbf{y}$ via (10) or (18), depending on the assumed graph smoothness prior, GLR or GTV, while the output embedding \mathbf{y}_i in a conventional transformer requires value matrix \mathbf{V} in (24). This also has a complexity implication.

5.3 Deep Algorithm Unrolling

We unroll T sequential pairs of an iterative interpolation algorithm (GLR- or GTV-based) with a graph learning module into an interpretable neural net. See Fig. 1a for an illustration of the GTV-based algorithm unrolling, where the t -th pair of ADMM block and the graph learning module have respective parameters Θ_t and Φ_t that are learned from back-propagation via a defined loss function. Φ_t include parameters used to define feature function $F(\cdot)$ and metric matrix \mathbf{M} in (25), so the module can construct a graph \mathcal{G} specified by incidence matrix \mathbf{C}^{t+1} given signal \mathbf{x}^t . In our implementation, we employ a shallow CNN to map a neighborhood of pixels centered at pixel i to a low-dimensional feature \mathbf{f}_i , with a parameter size smaller than query and key matrices, \mathbf{Q} and \mathbf{K} , in a conventional transformer. See Section 6.1 for details.

An ADMM block contains multiple ADMM layers that are unrolled iterations of the iterative ADMM algorithm described in Section 4.2. Each ADMM layer updates the main variables \mathbf{x} , \mathbf{z} , \mathbf{q} , auxiliary variable $\tilde{\mathbf{q}}$, and Lagrange multiplier $\boldsymbol{\mu}$ in turn using (17) to (22). ADMM weight parameter γ , as well as parameters in CG used to computed linear system (18), are learned via back-propagation. Specifically, two CG parameters α and β that represent step size and momentum during the conjugate gradient descent step are learned. See Appendix A.7 for details.

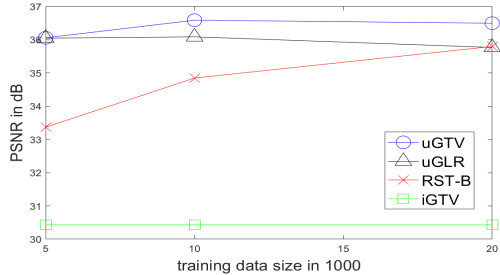


Figure 2: Demosaicking performance vs. training size for different models.

Method	Params #	McM PSNR	Kodak PSNR	Urban100 PSNR
RST-B	931763	34.85	38.75	32.82
RST-S	3162211	35.84	39.81	33.87
iGTV	-	30.43	28.66	24.91
uGLR	323410	36.09	37.88	33.60
uGTV	323435	36.59	39.11	34.01

Table 1: Demosaicking performance for models including SOTA RST-B (72 channels) and RST-S (96 channels) [45], trained on 10k sample dataset.

Method	McM PSNR			
	$\sigma = 10$	$\sigma = 20$	$\sigma = 30$	$\sigma = 50$
RST-B	28.01	22.7	19.34	15.03
uGLR	28.24	22.84	19.49	15.203
uGTV	28.31	22.89	19.56	15.38

Table 2: Demosaicking performance in noisy scenario, where models are trained on noiseless dataset.

Method	Params #	McM PSNR	Kodak PSNR	Urban100 PSNR
MAIN	10942977	32.72	28.23	25.46
iGTV	-	30.41	28.05	24.26
uGLR	323410	33.31	29.10	25.94
uGTV	323435	33.36	29.08	26.12

Table 3: Interpolation performance for models including SOTA MAIN [46], trained on 10k sample dataset.

6 Experiments

6.1 Experimental Setup

All models were developed using Python 3.11. We leveraged PyTorch to implement all models and trained them on an NVIDIA GeForce RTX 2080 Ti. To train each learned model, we used the DIV2K dataset, which contains 800 and 100 high-resolution (HR) training and validation images, respectively. Since the images are HR, we patchified the images into small images and used only about 1 to 4% of the patches for training and validation sets. We randomly sampled patches of 64×64 pixels to train the model. To test a model, we used the McM [42], Kodak [43], and Urban100 [44] datasets, running each model on the whole images. See Appendix A.8 for more implementation details.

We test model performance in two imaging applications: demosaicking and image interpolation. Demosaicking reconstructs a full-color image (each pixel contains RGB colors) from a Bayer-patterned image, where each pixel location has only one of Red, Green, or Blue. Interpolation reconstructs empty pixels missing all three colors in an image. To create input images, for the first application, we started from a full-color image and then removed color components per pixel according to the Bayer pattern. For the second application, we directly down-sampled horizontally and vertically a HR image by a factor of 2 to get the corresponding low-resolution (LR) image without any anti-aliasing filtering. This is equivalent to keeping every four pixels in the HR image.

6.2 Experimental Results

For the first application, we evaluate our graph-based models against two variants of RSTCANet [45], RSTCANet-B and RSTCANet-S (RST-B and RST-S for short), a SOTA framework that employs a swin transformer architecture. The baseline for our second application is MAIN [46], a multi-scale deep learning framework for image interpolation. We use Peak Signal-to-Noise Ratio (PSNR) as our evaluation metric, common in image quality assessment.

Table 1 shows the demosaicking performance for different models, where all models were trained on the same dataset and the same number of epochs (30), using a subset of DIV2K dataset containing $10K$ of 64×64 patches. We observe that our unrolled GTV model (uGTV) achieved the best overall performance, while the unrolled GLR model (uGLR) and RST-S performed similarly. Both our models (uGTV and uGLR) performed better than RST-B while employing significantly fewer parameters. The iterative GTV algorithm (iGTV) without parameter optimization performed the worst, demonstrating the importance of parameter learning. In Fig. 2, we see the demosaicking performance of different models versus training data size. We see that for small data size, our models

(uGTV and uGLR) performed significantly better than RST-B. This is intuitive, since a model with more parameters requires more training data in general. See Appendix A.9 for example visual results.

Next, we test robustness to covariate shift by testing models trained on noiseless data using a dataset artificially injected with Gaussian noise. Table 2 shows the demosaicking performance versus different noise variances. We observe that our models outperformed RST-B in all noisy scenarios.

For image interpolation, we interpolated a LR image to a corresponding HR image. We trained all models on the same dataset as the first application with the same number of epochs (15). Table 3 shows that under the same training conditions, our proposed models (uGTV and uGLR) outperformed MAIN in interpolation performance in all three benchmark datasets by about 0.7 dB. Note that for this application we only interpolated Y-channel from YCbCr color space for PSNR computation. Similar to the first application, our models achieved slight performance gain while employing drastically fewer parameters; specifically, uGTV employed only about 3% of the parameters in MAIN.

7 Conclusion

By unrolling iterative algorithms that minimize one of two graph smoothness priors— ℓ_2 -norm graph Laplacian regularizer (GLR) or ℓ_1 -norm graph total variation (GTV)—we build interpretable and light-weight transformer-like neural nets for the signal interpolation problem. The key insight is that the normalized graph learning module is akin to the self-attention mechanism in a conventional transformer architecture. Moreover, the interpolated signal in each layer is simply the low-pass filtered output derived from the assumed graph smoothness prior, eliminating the need for the value matrix. Experiments in two imaging applications show that interpolation results on par with SOTA can be achieved with a fraction of the parameters used in conventional transformers.

References

- [1] Dzmitry Bahdanau, Kyunghyun Cho, and Yoshua Bengio, “Neural machine translation by jointly learning to align and translate,” *CoRR*, vol. abs/1409.0473, 2014.
- [2] Ashish Vaswani, Noam Shazeer, Niki Parmar, Jakob Uszkoreit, Llion Jones, Aidan N Gomez, Lukasz Kaiser, and Illia Polosukhin, “Attention is all you need,” *Advances in neural information processing systems*, vol. 30, 2017.
- [3] Ze Liu, Yutong Lin, Yue Cao, Han Hu, Yixuan Wei, Zheng Zhang, Stephen Lin, and Baining Guo, “Swin transformer: Hierarchical vision transformer using shifted windows,” in *2021 IEEE/CVF International Conference on Computer Vision (ICCV)*, 2021, pp. 9992–10002.
- [4] Alexander Kolesnikov, Alexey Dosovitskiy, Dirk Weissenborn, Georg Heigold, Jakob Uszkoreit, Lucas Beyer, Matthias Minderer, Mostafa Dehghani, Neil Houlsby, Sylvain Gelly, Thomas Unterthiner, and Xiaohua Zhai, “An image is worth 16x16 words: Transformers for image recognition at scale,” in *The Ninth International Conference on Learning Representations (ICLR)*, 2021.
- [5] James Vuckovic, Aristide Baratin, and Rémi Tachet des Combes, “A mathematical theory of attention,” *ArXiv*, vol. abs/2007.02876, 2020.
- [6] Jingzhao Zhang, Sai Praneeth Karimireddy, Andreas Veit, Seungyeon Kim, Sashank Reddi, Sanjiv Kumar, and Suvrit Sra, “Why are adaptive methods good for attention models?,” in *Advances in Neural Information Processing Systems*, H. Larochelle, M. Ranzato, R. Hadsell, M.F. Balcan, and H. Lin, Eds. 2020, vol. 33, pp. 15383–15393, Curran Associates, Inc.
- [7] Charles Burton Snell, Ruiqi Zhong, Dan Klein, and Jacob Steinhardt, “Approximating how single head attention learns,” *ArXiv*, vol. abs/2103.07601, 2021.
- [8] Colin Wei, Yining Chen, and Tengyu Ma, “Statistically meaningful approximation: a case study on approximating turing machines with transformers,” in *Advances in Neural Information Processing Systems*, S. Koyejo, S. Mohamed, A. Agarwal, D. Belgrave, K. Cho, and A. Oh, Eds. 2022, vol. 35, pp. 12071–12083, Curran Associates, Inc.
- [9] Hyunjik Kim, George Papamakarios, and Andriy Mnih, “The lipschitz constant of self-attention,” in *Proceedings of the 38th International Conference on Machine Learning*, Marina Meila and Tong Zhang, Eds. 18–24 Jul 2021, vol. 139 of *Proceedings of Machine Learning Research*, pp. 5562–5571, PMLR.

- [10] Benjamin L Edelman, Surbhi Goel, Sham Kakade, and Cyril Zhang, “Inductive biases and variable creation in self-attention mechanisms,” in *Proceedings of the 39th International Conference on Machine Learning*, Kamalika Chaudhuri, Stefanie Jegelka, Le Song, Csaba Szepesvari, Gang Niu, and Sivan Sabato, Eds. 17–23 Jul 2022, vol. 162 of *Proceedings of Machine Learning Research*, pp. 5793–5831, PMLR.
- [11] Hongkang Li, Meng Wang, Sijia Liu, and Pin-Yu Chen, “A theoretical understanding of shallow vision transformers: Learning, generalization, and sample complexity,” in *The Eleventh International Conference on Learning Representations*, 2023.
- [12] Mostafa Dehghani, Josip Djolonga, Basil Mustafa, Piotr Padlewski, Jonathan Heek, Justin Gilmer, Andreas Peter Steiner, Mathilde Caron, Robert Geirhos, Ibrahim Alabdulmohsin, Rodolphe Jenatton, Lucas Beyer, Michael Tschannen, Anurag Arnab, Xiao Wang, Carlos Riquelme Ruiz, Matthias Minderer, Joan Puigcerver, Utku Evci, Manoj Kumar, Sjoerd Van Steenkiste, Gamaleldin Fathy Elsayed, Aravindh Mahendran, Fisher Yu, Avital Oliver, Fantine Huot, Jasmijn Bastings, Mark Collier, Alexey A. Gritsenko, Vignesh Birodkar, Cristina Nader Vasconcelos, Yi Tay, Thomas Mensink, Alexander Kolesnikov, Filip Pavetic, Dustin Tran, Thomas Kipf, Mario Lucic, Xiaohua Zhai, Daniel Keysers, Jeremiah J. Harmsen, and Neil Houlsby, “Scaling vision transformers to 22 billion parameters,” in *Proceedings of the 40th International Conference on Machine Learning*, Andreas Krause, Emma Brunskill, Kyunghyun Cho, Barbara Engelhardt, Sivan Sabato, and Jonathan Scarlett, Eds. 23–29 Jul 2023, vol. 202 of *Proceedings of Machine Learning Research*, pp. 7480–7512, PMLR.
- [13] Ruiqi Zhang, Spencer Frei, and Peter L. Bartlett, “Trained transformers learn linear models in-context,” *Journal of Machine Learning Research*, vol. 25, no. 49, pp. 1–55, 2024.
- [14] Vishal Monga, Yuelong Li, and Yonina C. Eldar, “Algorithm unrolling: Interpretable, efficient deep learning for signal and image processing,” *IEEE Signal Processing Magazine*, vol. 38, no. 2, pp. 18–44, 2021.
- [15] Karol Gregor and Yann LeCun, “Learning fast approximations of sparse coding,” in *Proceedings of the 27th International Conference on International Conference on Machine Learning*, Madison, WI, USA, 2010, ICML’10, p. 399–406, Omnipress.
- [16] Yaodong Yu, Sam Buchanan, Druv Pai, Tianzhe Chu, Ziyang Wu, Shengbang Tong, Benjamin Haeffele, and Yi Ma, “White-box transformers via sparse rate reduction,” in *Advances in Neural Information Processing Systems*, A. Oh, T. Neumann, A. Globerson, K. Saenko, M. Hardt, and S. Levine, Eds. 2023, vol. 36, pp. 9422–9457, Curran Associates, Inc.
- [17] D. I. Shuman, S. K. Narang, P. Frossard, A. Ortega, and P. Vandergheynst, “The emerging field of signal processing on graphs: Extending high-dimensional data analysis to networks and other irregular domains,” in *IEEE Signal Processing Magazine*, May 2013, vol. 30, no.3, pp. 83–98.
- [18] A. Ortega, P. Frossard, J. Kovacevic, J. M. F. Moura, and P. Vandergheynst, “Graph signal processing: Overview, challenges, and applications,” in *Proceedings of the IEEE*, May 2018, vol. 106, no.5, pp. 808–828.
- [19] G. Cheung, E. Magli, Y. Tanaka, and M. Ng, “Graph spectral image processing,” in *Proceedings of the IEEE*, May 2018, vol. 106, no.5, pp. 907–930.
- [20] J. Pang and G. Cheung, “Graph Laplacian regularization for inverse imaging: Analysis in the continuous domain,” in *IEEE Transactions on Image Processing*, April 2017, vol. 26, no.4, pp. 1770–1785.
- [21] X. Liu, G. Cheung, X. Wu, and D. Zhao, “Random walk graph Laplacian based smoothness prior for soft decoding of JPEG images,” *IEEE Transactions on Image Processing*, vol. 26, no.2, pp. 509–524, February 2017.
- [22] Fei Chen, Gene Cheung, and Xue Zhang, “Manifold graph signal restoration using gradient graph Laplacian regularizer,” *IEEE Transactions on Signal Processing*, vol. 72, pp. 744–761, 2024.
- [23] Jin Zeng, Jiahao Pang, Wenxiu Sun, and Gene Cheung, “Deep graph Laplacian regularization for robust denoising of real images,” in *2019 IEEE/CVF Conference on Computer Vision and Pattern Recognition Workshops (CVPRW)*, 2019, pp. 1759–1768.
- [24] Chinthaka Dinesh, Gene Cheung, and Ivan V. Bajić, “Point cloud denoising via feature graph laplacian regularization,” *IEEE Transactions on Image Processing*, vol. 29, pp. 4143–4158, 2020.

- [25] Chinthaka Dinesh, Gene Cheung, and Ivan V. Bajić, “Point cloud video super-resolution via partial point coupling and graph smoothness,” *IEEE Transactions on Image Processing*, vol. 31, pp. 4117–4132, 2022.
- [26] Wei Hu, Xiang Gao, Gene Cheung, and Zongming Guo, “Feature graph learning for 3D point cloud denoising,” *IEEE Transactions on Signal Processing*, vol. 68, pp. 2841–2856, 2020.
- [27] Cheng Yang, Gene Cheung, and Wei Hu, “Signed graph metric learning via Gershgorin disc perfect alignment,” *IEEE Transactions on Pattern Analysis and Machine Intelligence*, vol. 44, no. 10, pp. 7219–7234, 2022.
- [28] Abderrahim Elmoataz, Olivier Lezoray, and Sébastien Bouteau, “Nonlocal discrete regularization on weighted graphs: A framework for image and manifold processing,” *IEEE Transactions on Image Processing*, vol. 17, no. 7, pp. 1047–1060, 2008.
- [29] Camille Couprie, Leo Grady, Laurent Najman, Jean-Christophe Pesquet, and Hugues Talbot, “Dual constrained tv-based regularization on graphs,” *SIAM Journal on Imaging Sciences*, vol. 6, no. 3, pp. 1246–1273, 2013.
- [30] Peter Berger, Gabor Hannak, and Gerald Matz, “Graph signal recovery via primal-dual algorithms for total variation minimization,” *IEEE Journal of Selected Topics in Signal Processing*, vol. 11, no. 6, pp. 842–855, 2017.
- [31] J. R. Shewchuk, “An introduction to the conjugate gradient method without the agonizing pain,” Tech. Rep., USA, 1994.
- [32] Sinong Wang and Ness Shroff, “A new alternating direction method for linear programming,” in *Advances in Neural Information Processing Systems*, I. Guyon, U. Von Luxburg, S. Bengio, H. Wallach, R. Fergus, S. Vishwanathan, and R. Garnett, Eds. 2017, vol. 30, Curran Associates, Inc.
- [33] Y. Bai, G. Cheung, X. Liu, and W. Gao, “Graph-based blind image deblurring from a single photograph,” *IEEE Transactions on Image Processing*, vol. 28, no.3, pp. 1404–1418, 2019.
- [34] S. Boyd and L. Vandenberghe, *Convex Optimization*, Cambridge, 2004.
- [35] G. Golub and C. F. Van Loan, *Matrix Computations (Johns Hopkins Studies in the Mathematical Sciences)*, Johns Hopkins University Press, 2012.
- [36] E. Brian Davies, Graham M. L. Gladwell, Josef Leydold, Peter F. Stadler, and Peter F. Stadler, “Discrete nodal domain theorems,” *Linear Algebra and its Applications*, vol. 336, pp. 51–60, 2000.
- [37] S. Boyd, N. Parikh, E. Chu, B. Peleato, and J. Eckstein, “Distributed optimization and statistical learning via the alternating direction method of multipliers,” in *Foundations and Trends in Optimization*, 2011, vol. 3, no.1, pp. 1–122.
- [38] H. Egilmez, E. Pavez, and A. Ortega, “Graph learning from data under Laplacian and structural constraints,” in *IEEE Journal of Selected Topics in Signal Processing*, July 2017, vol. 11, no.6, pp. 825–841.
- [39] Xiaowen Dong, Dorina Thanou, Michael Rabbat, and Pascal Frossard, “Learning graphs from data: A signal representation perspective,” *IEEE Signal Processing Magazine*, vol. 36, no. 3, pp. 44–63, 2019.
- [40] Saghar Bagheri, Gene Cheung, Antonio Ortega, and Fen Wang, “Learning sparse graph Laplacian with K eigenvector prior via iterative Glasso and projection,” in *ICASSP 2021 - 2021 IEEE International Conference on Acoustics, Speech and Signal Processing (ICASSP)*, 2021, pp. 5365–5369.
- [41] C. Tomasi and R. Manduchi, “Bilateral filtering for gray and color images,” in *Proceedings of the IEEE International Conference on Computer Vision*, Bombay, India, 1998.
- [42] Lei Zhang, Xiaolin Wu, Antoni Buades, and Xin Li, “Color demosaicking by local directional interpolation and nonlocal adaptive thresholding,” *Journal of Electronic imaging*, vol. 20, no. 2, pp. 023016–023016, 2011.
- [43] Eastman Kodak, “Kodak lossless true color image suite (photocd pcd0992),” URL <http://r0k.us/graphics/kodak>, vol. 6, pp. 2, 1993.

- [44] Jia-Bin Huang, Abhishek Singh, and Narendra Ahuja, “Single image super-resolution from transformed self-exemplars,” in *Proceedings of the IEEE conference on computer vision and pattern recognition*, 2015, pp. 5197–5206.
- [45] Wenzhu Xing and Karen Egiazarian, “Residual swin transformer channel attention network for image demosaicing,” in *2022 10th European Workshop on Visual Information Processing (EUVIP)*. IEEE, 2022, pp. 1–6.
- [46] Jiahuan Ji, Baojiang Zhong, and Kai-Kuang Ma, “Image interpolation using multi-scale attention-aware inception network,” *IEEE Transactions on Image Processing*, vol. 29, pp. 9413–9428, 2020.
- [47] Yurii Nesterov, *Introductory lectures on convex optimization: A basic course*, vol. 87, Springer Science & Business Media, 2013.

A Appendix

A.1 Full-Rankness of Matrix \mathbf{P} in (4)

Given that the underlying graph \mathcal{G} is positive and connected, we prove that coefficient matrix \mathbf{P} in (4) is full-rank and thus invertible. We prove by contradiction: suppose \mathbf{P} is *not* full-rank, and there exists a vector $\mathbf{v} = [\mathbf{x}; \boldsymbol{\mu}]$ such that $\mathbf{P}\mathbf{v} = \mathbf{0}_{N+K}$. Suppose we order K sampled entries \mathbf{x}_S before $N - K$ non-sampled entries $\mathbf{x}_{\bar{S}}$ in \mathbf{x} , *i.e.*, $\mathbf{x} = [\mathbf{x}_S; \mathbf{x}_{\bar{S}}]$. First, given sampling matrix $\mathbf{H} = [\mathbf{I}_K \ \mathbf{0}_{K, N-K}] \in \{0, 1\}^{K \times N}$, focusing on the second block row of \mathbf{P} , $[\mathbf{H} \ \mathbf{0}_{K, K}]\mathbf{v} = \mathbf{0}_K$ means $\mathbf{H}\mathbf{x} = [\mathbf{I}_K \ \mathbf{0}_{K, N-K}][\mathbf{x}_S; \mathbf{x}_{\bar{S}}] = \mathbf{0}_K$. Thus, sampled entries of \mathbf{x} must be zeros, *i.e.*, $\mathbf{x}_S = \mathbf{0}_K$.

Second, suppose we write Laplacian \mathbf{L} in blocks, *i.e.*, $\mathbf{L} = [\mathbf{L}_{S,S} \ \mathbf{L}_{S,\bar{S}}; \mathbf{L}_{\bar{S},S} \ \mathbf{L}_{\bar{S},\bar{S}}]$. Then, the non-sampled rows of the first block row of $\mathbf{M}\mathbf{v}$ are

$$\left([2\mathbf{L} \ \mathbf{H}^\top] \begin{bmatrix} \mathbf{x} \\ \boldsymbol{\mu} \end{bmatrix} \right)_{\bar{S}} = 2(\mathbf{L}_{\bar{S},S}\mathbf{x}_S + \mathbf{L}_{\bar{S},\bar{S}}\mathbf{x}_{\bar{S}}) \quad (27)$$

where $(\mathbf{H}^\top \boldsymbol{\mu})_{\bar{S}} = \mathbf{0}_{N-K}$ since non-sampled rows of $\mathbf{H}^\top = [\mathbf{I}_K; \mathbf{0}_{N-K, K}]$ are all zeros. From above, we know $\mathbf{x}_S = \mathbf{0}_K$, and thus $([2\mathbf{L} \ \mathbf{H}^\top]\mathbf{v})_{\bar{S}} = \mathbf{0}_{N-K}$ implies that we require $\mathbf{L}_{\bar{S},\bar{S}}\mathbf{x}_{\bar{S}} = \mathbf{0}_N$. However, since $\mathbf{L}_{\bar{S},\bar{S}}$ is a combinatorial Laplacian matrix for a positive sub-graph connecting non-sampled nodes *plus* at least one strictly positive self-loop (representing an edge from a non-sampled node to a sample node), given \mathcal{G} is a connected positive graph, $\mathbf{L}_{\bar{S},\bar{S}}$ must be PD (see Appendix A.2 below). Thus, $\nexists \mathbf{x}_{\bar{S}} \neq \mathbf{0}$ s.t. $\mathbf{L}_{\bar{S},\bar{S}}\mathbf{x}_{\bar{S}} = \mathbf{0}_{N-K}$, a contradiction. Therefore, we can conclude that \mathbf{P} must be full-rank.

A.2 Positive Definiteness of Matrix $\mathbf{L}_{\bar{S},\bar{S}}$ in (8)

Given that the underlying graph \mathcal{G} is positive and connected, we prove that coefficient matrix $\mathbf{L}_{\bar{S},\bar{S}}$ in (8) is PD. By definition $\mathbf{L} \triangleq \text{diag}(\mathbf{W}\mathbf{1}_N) - \mathbf{W}$, where \mathbf{W} is an adjacency matrix for a positive graph without self-loops, *i.e.*, $W_{i,j} \geq 0, \forall i \neq j$ and $W_{i,i} = 0, \forall i$. Thus, $L_{i,i} = \sum_j W_{i,j}, \forall i$, and $L_{i,j} = -W_{i,j} \leq 0, \forall i \neq j$. For sub-matrix $\mathbf{L}_{\bar{S},\bar{S}}$, $L_{i,i} = \sum_{j \in \bar{S}} W_{i,j} + \sum_{j \in S} W_{i,j}, \forall i \in \bar{S}$. Define $\mathbf{L}'_{\bar{S},\bar{S}}$ as a graph Laplacian matrix for nodes in \bar{S} considering only edges between nodes in \bar{S} , *i.e.*, $L_{i,i} = \sum_{j \in \bar{S}} W_{i,j}, \forall i \in \bar{S}$. Define $\mathbf{D}'_{\bar{S},\bar{S}}$ as a diagonal degree matrix for nodes in \bar{S} considering only edges between \bar{S} and S , *i.e.*, $D'_{i,i} = \sum_{j \in S} W_{i,j}, \forall i \in \bar{S}$. Note that $D'_{i,i} \geq 0, \forall i$. We can now write $\mathbf{L}_{\bar{S},\bar{S}}$ as

$$\mathbf{L}_{\bar{S},\bar{S}} = \mathbf{L}'_{\bar{S},\bar{S}} + \mathbf{D}'_{\bar{S},\bar{S}}. \quad (28)$$

$\mathbf{L}'_{\bar{S},\bar{S}}$ is a combinatorial graph Laplacian for a positive graph without self-loops, and thus is provably PSD [19]. $\mathbf{D}'_{\bar{S},\bar{S}}$ is a non-negative diagonal matrix, and thus is also PSD. By Weyl's inequality, $\mathbf{L}_{\bar{S},\bar{S}}$ is also PSD.

We prove by contradiction: suppose $\mathbf{L}_{\bar{S},\bar{S}}$ is not PD, and $\exists \mathbf{x} \neq \mathbf{0}$ such that $\mathbf{x}^\top \mathbf{L}_{\bar{S},\bar{S}} \mathbf{x} = 0$. $\mathbf{x}^\top \mathbf{L}_{\bar{S},\bar{S}} \mathbf{x} = 0$ iff $\mathbf{x}^\top \mathbf{L}'_{\bar{S},\bar{S}} \mathbf{x} = 0$ and $\mathbf{x}^\top \mathbf{D}'_{\bar{S},\bar{S}} \mathbf{x} = 0$ simultaneously. Denote by \bar{S}_1 and \bar{S}_2 the indices of nodes in \bar{S} with and without connections to nodes in S , respectively. $\bar{S}_1 \neq \emptyset$, since \mathcal{G} is connected. Suppose first $\bar{S}_2 = \emptyset$. Then $\mathbf{D}'_{\bar{S},\bar{S}}$ has strictly positive diagonal entries and is PD, and there is no $\mathbf{x} \neq \mathbf{0}$ s.t. $\mathbf{x}^\top \mathbf{D}'_{\bar{S},\bar{S}} \mathbf{x} = 0$, a contradiction.

Suppose now $\bar{S}_2 \neq \emptyset$. First, $\mathbf{x}^\top \mathbf{D}'_{\bar{S},\bar{S}} \mathbf{x} = 0$ implies $\mathbf{x}_{\bar{S}_1} = \mathbf{0}$. Then,

$$\mathbf{x}^\top \mathbf{L}'_{\bar{S},\bar{S}} \mathbf{x} = \sum_{i,j \in \bar{S}} W_{i,j} (x_i - x_j)^2 \geq \sum_{i \in \bar{S}_1, j \in \bar{S}_2} W_{i,j} (x_i - x_j)^2. \quad (29)$$

Since each term in the sum is non-negative, the sum is zero only if for each $(i, j) \in \mathcal{E}$ where $i \in \bar{S}_1$ and $j \in \bar{S}_2$, $0 = x_i = x_j$. For nodes $k \in \bar{S}_2$ connected only to nodes $j \in \bar{S}_2$ connected to $i \in \bar{S}_1$, $x_k = x_j = x_i = 0$ necessarily, and for nodes $l \in \bar{S}_2$ connected to $k \in \bar{S}_2$ must have $x_l = x_k = 0$, and so on. Thus, $\mathbf{x} = \mathbf{0}$, a contradiction. Thus, we can conclude that $\mathbf{L}_{\bar{S},\bar{S}}$ is PD.

A.3 Derivation of (17), (18) and (19)

We define $\phi = [\mathbf{z}; \mathbf{x}; \mathbf{q}_1; \mathbf{q}_2]$ and rewrite the objective (16) to

$$\begin{aligned} \min_{\phi} & \begin{bmatrix} \mathbf{1}_M \\ \mathbf{0}_{N+2M} \end{bmatrix}^\top \phi + (\boldsymbol{\mu}^t)^\top \left(\begin{bmatrix} \mathbf{A} \\ \mathbf{0}_{2M, M+N} \ \mathbf{I}_{2M} \end{bmatrix} \phi - \begin{bmatrix} \mathbf{b} \\ \tilde{\mathbf{q}}^t \end{bmatrix} \right) \\ & + \frac{\gamma}{2} \left\| \underbrace{\begin{bmatrix} \mathbf{A} \\ \mathbf{0}_{2M, M+N} \ \mathbf{I}_{2M} \end{bmatrix}}_{\mathbf{B}} \phi - \begin{bmatrix} \mathbf{b} \\ \tilde{\mathbf{q}}^t \end{bmatrix} \right\|_2^2. \end{aligned} \quad (30)$$

(30) is a convex quadratic objective, and so we take the derivative w.r.t. ϕ and set it to $\mathbf{0}$:

$$\begin{aligned} & \begin{bmatrix} \mathbf{1}_M \\ \mathbf{0}_{N+2M} \end{bmatrix} + \begin{bmatrix} \mathbf{A}^\top & \mathbf{0}_{M+N, 2M} \\ & \mathbf{I}_{2M} \end{bmatrix} (\boldsymbol{\mu}^t) \\ & + \frac{\gamma}{2} \left(2 \begin{bmatrix} \mathbf{A}^\top & \mathbf{0}_{M+N, 2M} \\ & \mathbf{I}_{2M} \end{bmatrix} \begin{bmatrix} \mathbf{A} \\ \mathbf{0}_{2M, M+N} \ \mathbf{I}_{2M} \end{bmatrix} \phi - 2 \begin{bmatrix} \mathbf{A}^\top & \mathbf{0}_{M+N, 2M} \\ & \mathbf{I}_{2M} \end{bmatrix} \begin{bmatrix} \mathbf{b} \\ \tilde{\mathbf{q}}^t \end{bmatrix} \right) = \mathbf{0}. \end{aligned} \quad (31)$$

Given that \mathbf{B} is the following matrix:

$$\mathbf{B} = \begin{bmatrix} \mathbf{I}_M & -\mathbf{C} & -\mathbf{I}_M & \mathbf{0}_M \\ \mathbf{I}_M & \mathbf{C} & \mathbf{0}_M & -\mathbf{I}_M \\ \mathbf{0}_{K, M} & \mathbf{H} & \mathbf{0}_{K, M} & \mathbf{0}_{K, M} \\ \mathbf{0}_{M, M} & \mathbf{0}_{M, N} & \mathbf{I}_M & \mathbf{0}_M \\ \mathbf{0}_{M, M} & \mathbf{0}_{M, N} & \mathbf{0}_M & \mathbf{I}_M \end{bmatrix} \quad (32)$$

Hence, $\mathbf{B}^\top \mathbf{B}$ is

$$\mathbf{B}^\top \mathbf{B} = \begin{bmatrix} 2\mathbf{I}_M & \mathbf{0}_{M, N} & -\mathbf{I}_M & -\mathbf{I}_M \\ \mathbf{0}_{N, M} & 2\mathbf{C}^\top \mathbf{C} + \mathbf{H}^\top \mathbf{H} & \mathbf{C}^\top & -\mathbf{C}^\top \\ -\mathbf{I}_M & \mathbf{C} & 2\mathbf{I}_M & \mathbf{0}_{M, M} \\ -\mathbf{I}_M & -\mathbf{C} & \mathbf{0}_{M, M} & 2\mathbf{I}_M \end{bmatrix}. \quad (33)$$

Note that adding two of row 1 to rows 3 and 4, we get $[2\mathbf{I}_M \ \mathbf{0}_{M, N} \ \mathbf{0}_{M, M} \ \mathbf{0}_{M, M}]$.

Solving for ϕ in (31), we get

$$\gamma \mathbf{B}^\top \mathbf{B} \phi = - \begin{bmatrix} \mathbf{1}_M \\ \mathbf{0}_N \\ \mathbf{0}_M \\ \mathbf{0}_M \end{bmatrix} - \mathbf{B}^\top \left(\begin{bmatrix} \boldsymbol{\mu}_a^t \\ \boldsymbol{\mu}_b^t \\ \boldsymbol{\mu}_c^t \\ \boldsymbol{\mu}_d^t \\ \boldsymbol{\mu}_e^t \end{bmatrix} - \gamma \begin{bmatrix} \mathbf{0}_M \\ \mathbf{0}_M \\ \mathbf{y} \\ \tilde{\mathbf{q}}_1^t \\ \tilde{\mathbf{q}}_2^t \end{bmatrix} \right) \quad (34)$$

$$= \begin{bmatrix} -\mathbf{1}_M - \boldsymbol{\mu}_a^t - \boldsymbol{\mu}_b^t \\ \mathbf{C}^\top \boldsymbol{\mu}_a^t - \mathbf{C}^\top \boldsymbol{\mu}_b^t - \mathbf{H}^\top \boldsymbol{\mu}_c^t + \gamma \mathbf{H}^\top \mathbf{y} \\ \boldsymbol{\mu}_a^t - \boldsymbol{\mu}_d^t + \gamma \tilde{\mathbf{q}}_1^t \\ \boldsymbol{\mu}_b^t - \boldsymbol{\mu}_e^t + \gamma \tilde{\mathbf{q}}_2^t \end{bmatrix} \quad (35)$$

We can solve for \mathbf{z}^{t+1} directly; by adding two of row 1 to rows 3 and 4 of (35), we get

$$\begin{aligned} 2\gamma \mathbf{z}^{t+1} &= -2(\mathbf{1}_M) - \boldsymbol{\mu}_a^t - \boldsymbol{\mu}_b^t - \boldsymbol{\mu}_d^t - \boldsymbol{\mu}_e^t + \gamma(\tilde{\mathbf{q}}_1^t + \tilde{\mathbf{q}}_2^t) \\ \mathbf{z}^{t+1} &= -\frac{1}{\gamma} \mathbf{1}_M - \frac{1}{2\gamma} (\boldsymbol{\mu}_a^t + \boldsymbol{\mu}_b^t + \boldsymbol{\mu}_d^t + \boldsymbol{\mu}_e^t) + \frac{1}{2} (\tilde{\mathbf{q}}_1^t + \tilde{\mathbf{q}}_2^t). \end{aligned} \quad (36)$$

Subtracting row 4 from row 3 of (35), we get

$$\begin{aligned} 2\gamma \mathbf{C} \mathbf{x}^{t+1} + 2\gamma (\mathbf{q}_1^{t+1} - \mathbf{q}_2^{t+1}) &= \boldsymbol{\mu}_a^t - \boldsymbol{\mu}_b^t - \boldsymbol{\mu}_d^t + \boldsymbol{\mu}_e^t + \gamma(\tilde{\mathbf{q}}_1^t - \tilde{\mathbf{q}}_2^t) \\ \gamma (\mathbf{q}_1^{t+1} - \mathbf{q}_2^{t+1}) &= -\gamma \mathbf{C} \mathbf{x}^{t+1} + \frac{1}{2} (\boldsymbol{\mu}_a^t - \boldsymbol{\mu}_b^t - \boldsymbol{\mu}_d^t + \boldsymbol{\mu}_e^t) + \frac{\gamma}{2} (\tilde{\mathbf{q}}_1^t - \tilde{\mathbf{q}}_2^t). \end{aligned} \quad (37)$$

Thus, row 2 can be rewritten as

$$\begin{aligned} \gamma(2\mathbf{C}^\top\mathbf{C} + \mathbf{H}^\top\mathbf{H})\mathbf{x}^{t+1} + \mathbf{C}^\top\gamma(\mathbf{q}_1^{t+1} - \mathbf{q}_2^{t+1}) &= \mathbf{C}^\top\boldsymbol{\mu}_a^t - \mathbf{C}^\top\boldsymbol{\mu}_b^t - \mathbf{H}^\top\boldsymbol{\mu}_c^t + \gamma\mathbf{H}^\top\mathbf{y} \\ \gamma(\mathbf{C}^\top\mathbf{C} + \mathbf{H}^\top\mathbf{H})\mathbf{x}^{t+1} &= \frac{1}{2}\mathbf{C}^\top(\boldsymbol{\mu}_a^t - \boldsymbol{\mu}_b^t + \boldsymbol{\mu}_d^t - \boldsymbol{\mu}_e^t) - \mathbf{H}^\top\boldsymbol{\mu}_c^t \\ &\quad - \frac{\gamma}{2}\mathbf{C}^\top(\tilde{\mathbf{q}}_1^t - \tilde{\mathbf{q}}_2^t) + \gamma\mathbf{H}^\top\mathbf{y}. \end{aligned} \quad (38)$$

Finally, from rows 3 and 4, \mathbf{q}_1^t and \mathbf{q}_2^t can be computed as

$$\begin{aligned} \mathbf{q}_1^t &= \frac{1}{2}(\mathbf{z}^{t+1} - \mathbf{C}\mathbf{x}^{t+1}) + \frac{1}{2\gamma}(\boldsymbol{\mu}_a^t - \boldsymbol{\mu}_d^t + \gamma\tilde{\mathbf{q}}_1^t) \\ \mathbf{q}_2^t &= \frac{1}{2}(\mathbf{z}^{t+1} + \mathbf{C}\mathbf{x}^{t+1}) + \frac{1}{2\gamma}(\boldsymbol{\mu}_b^t - \boldsymbol{\mu}_e^t + \gamma\tilde{\mathbf{q}}_2^t). \end{aligned} \quad (39)$$

A.4 Invertibility of $\mathcal{L} = \mathbf{C}^\top\mathbf{C} + \mathbf{H}^\top\mathbf{H}$

Clearly $\mathcal{L} = \mathbf{C}^\top\mathbf{C} + \mathbf{H}^\top\mathbf{H}$ is real, symmetric, and positive semi-definite. Thus its eigenvalues are real and non-negative. To show that it is invertible, it suffices to show that its minimum eigenvalue $\lambda_{\min}(\mathcal{L})$ is strictly greater than zero. But $\lambda_{\min}(\mathcal{L}) = \min_{\mathbf{x}: \|\mathbf{x}\|=1} \mathbf{x}^\top\mathcal{L}\mathbf{x}$. Hence it suffices to show that $\mathbf{x}^\top\mathcal{L}\mathbf{x} = 0$ implies $\mathbf{x} = \mathbf{0}$. Now observe that $\mathbf{x}^\top\mathcal{L}\mathbf{x} = \sum_{(i,j) \in \mathcal{E}} w_{i,j}^2 (x_i - x_j)^2 + \sum_{i \in \mathcal{S}} x_i^2$, where \mathcal{S} is the set of nodes with constrained values. If $\mathbf{x}^\top\mathcal{L}\mathbf{x} = 0$ then all terms must be zero, meaning that all x_i in \mathcal{S} are zero, and hence all of their neighbors, and all of *their* neighbors, and so on. Thus, \mathcal{L} is invertible if there exists at least one node with a constrained value (i.e., a self-loop) in each connected component of the graph.

A.5 Derivation of (21)

We derive the solution to optimization (20). Ignoring the first convex but non-smooth term $g(\tilde{\mathbf{q}})$, the remaining two terms in the objective are convex and smooth. Taking the derivative w.r.t. variable $\tilde{\mathbf{q}}$ and setting it to $\mathbf{0}$, we get

$$\begin{aligned} -\boldsymbol{\mu}_d^t - \gamma\mathbf{q}^{t+1} + \gamma\tilde{\mathbf{q}}^* &= \mathbf{0}_M \\ \tilde{\mathbf{q}}^* &= \mathbf{q}^{t+1} + \frac{1}{\gamma}\boldsymbol{\mu}_d^t. \end{aligned} \quad (40)$$

This solution is valid iff $g(\tilde{\mathbf{q}}^*) = 0$; otherwise the first term $g(\tilde{\mathbf{q}}^*)$ dominates and $\tilde{\mathbf{q}}^* = \mathbf{0}_M$. Given that (40) can be computed entry-by-entry separately, (21) follows.

A.6 Example of Edge Weight Normalization for the Incidence Matrix

In Fig. 3(top), we show an example three-node *undirected* graph with three edge weights $w_{1,2} = 1/2$, $w_{1,3} = 1/2$, and $w_{2,3} = 1/3$, and the corresponding incidence matrix \mathbf{C} . Normalizing edge weights using (26), we see in Fig. 3(middle) a *directed* graph with six edges where the sum of normalized edge weights leaving a node is 1, resulting in normalized incidence matrix $\tilde{\mathbf{C}}$. Finally, we see in Fig. 3(bottom) an *undirected* graph with three edges corresponding to graph Laplacian $\tilde{\mathbf{L}} = \tilde{\mathbf{C}}^\top\tilde{\mathbf{C}}$. Note that $\|\tilde{\mathbf{C}}\mathbf{1}_3\|_1 = \mathbf{0}_6$ as expected.

A.7 Parameters Learning in Conjugate Gradient Algorithm (CG)

The linear systems that we need to solve—(8) for GLR minimization and (18) for GTV minimization—have the follow form,

$$\mathcal{L}\mathbf{x} = \mathbf{b}. \quad (41)$$

Given \mathcal{L} is PD, we consider the minimization problem,

$$\min_{\mathbf{x}} Q(\mathbf{x}) = \frac{1}{2}\mathbf{x}^\top\mathcal{L}\mathbf{x} - \mathbf{b}^\top\mathbf{x} \quad (42)$$

with gradient

$$\frac{\delta Q(\mathbf{x})}{\delta \mathbf{x}} = \mathcal{L}\mathbf{x} - \mathbf{b}. \quad (43)$$

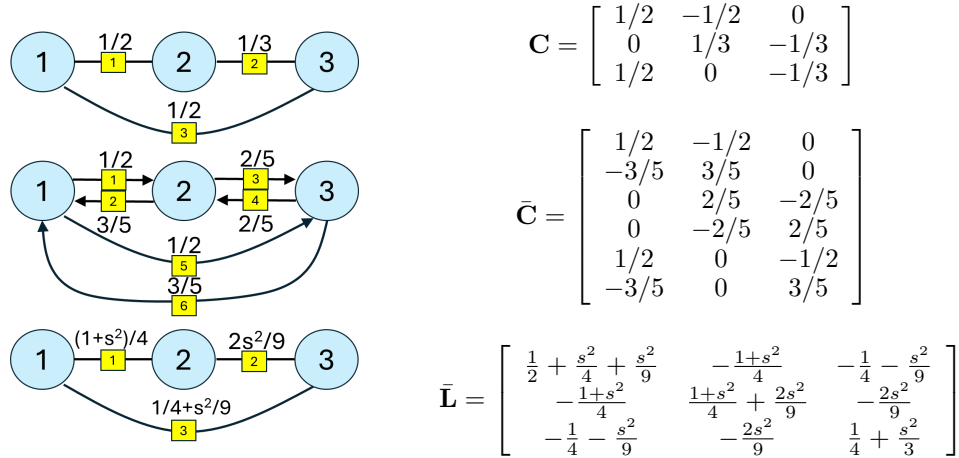


Figure 3: 3-node graph for incidence matrix \mathbf{C} (top), 3-node graph for normalized incidence matrix $\bar{\mathbf{C}}$ (middle), 3-node graph for graph Laplacian $\bar{\mathbf{L}} = \mathbf{C}^\top \bar{\mathbf{C}}$ where $s = \frac{6}{5}$ (bottom).

Thus, the simple gradient descent has the following update rules with α_t commonly known as learning rate,

$$\mathbf{g}^t = \mathcal{L}\mathbf{x}^t - \mathbf{b} = \mathbf{g}^{t-1} - \alpha_t \mathcal{L}\mathbf{g}^{t-1} \quad (44)$$

$$\mathbf{x}^{t+1} = \mathbf{x}^t - \alpha_t \mathbf{g}^t. \quad (45)$$

Next, a momentum term β_t and the cumulative gradients term \mathbf{v}^t are added, resulting in the well-known Accelerated Gradient Descent Algorithm [47], also known as Conjugated Gradient Descent. The new update rules are

$$\mathbf{g}^t = \mathbf{g}^{t-1} - \alpha_t \mathcal{L}\mathbf{v}^{t-1} \quad (46)$$

$$\mathbf{v}^t = \mathbf{g}^t + \beta_t \mathbf{v}^{t-1} \quad (47)$$

$$\mathbf{x}^{t+1} = \mathbf{x}^t - \alpha_t \mathbf{v}^t \quad (48)$$

where both α_t and β_t in each iteration t are considered trainable parameters.

A.8 Experimental Details

We first developed our unrolled ADMM model without training any parameters of the model. We first estimated the target signal \mathbf{x} using linear interpolation of known values in a 5×5 pixel neighborhood. We then used RGB values and pixel locations together to form feature vectors to compute edge weights $w_{i,j}$ and shared the weights for the three channels. We initialized metric matrix M as a diagonal matrix with all entries equal to 1.5. We initialized vectors $\mu_a, \mu_b, \mu_c, \mu_d,$ and μ_e to be vectors with all entries equal to 0.1. We set γ to 10 and α and β in CG to 0.5 and 0.3 respectively. For the learned ADMM block, we learned $\gamma, \alpha, \beta,$ and metric matrix M . We created our training dataset consist of 5000, 10000, or 20000 images patches of size 64×64 to train the model.

All matrix multiplications in our models are implemented to take advantage of the sparsity of the constructed graphs, which were restricted to be a window of size $5 \times 5 = 25$ nearest neighbors of each pixel. This ensures that our graphs are always *connected* and *sparse*. We stacked vertically 4 Graph Learning modules coupled with ADMM block, so that we can learn multiple graphs in parallel. This is commonly known as multi-head in the transformer architecture. We also stacked 5 graph learning modules and ADMM blocks horizontally to further learn more graphs. In all ADMM blocks, we set the number of ADMM iterations to 5 and the number of CG iterations to 10.

To extract high-level features, we employed a shallow CNN with 4 convolution layers with 48 feature maps (12 features for each graph learning head) followed by ReLU activation function after each convolution layer. 3×3 kernels were used with *no* down-sampling to produce 48 features for each pixel. We divided the feature maps into 4 sets; each becomes the input of the Graph Learning module to produce 4 graphs in parallel. Then a simple weighted average scheme was used to combine the

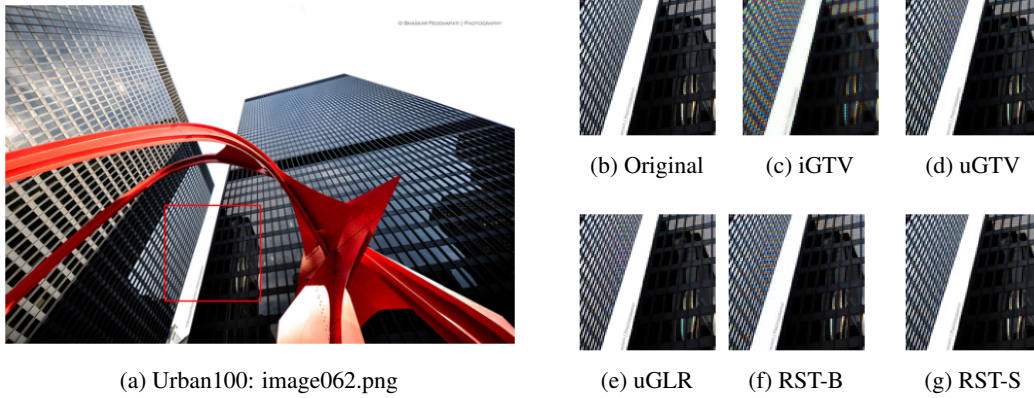


Figure 4: Visual demosaicking results for image *Urban062*.

outputs as one output x^t . We also added skip connections between convolution layers to ease the training process.

A.9 Additional Experimental Results

Fig. 4 shows visual results for a test image for all models, including our uGTV, uGLR and the baselines. Two variants of RSTCANet, uGTV and uGLR are trained on 10000 images patches of size 64×64 for 30 epochs. We observe that our two models, especially uGTV, has better performance compared to RST-B and comparable performance with RST-S in selected high-frequency area.